

# Interannual variability and climatic sensitivity of global wildfire activity

Rongyun TANG<sup>a,b</sup>, Jiafu MAO<sup>b,\*</sup>, Mingzhou JIN<sup>a</sup>, Anping CHEN<sup>c</sup>, Yan YU<sup>d</sup>, Xiaoying SHI<sup>b</sup>, Yulong ZHANG<sup>a</sup>, Forrest M. HOFFMAN<sup>e</sup>, Min XU<sup>e</sup>, Yaoping WANG<sup>a</sup>

<sup>a</sup> Institute for a Secure and Sustainable Environment, University of Tennessee, Knoxville, 37996, USA

<sup>b</sup> Environmental Sciences Division and Climate Change Science Institute, Oak Ridge National Laboratory, Oak Ridge, 37830, USA

<sup>c</sup> Department of Biology and Graduate Degree Program in Ecology, Colorado State University, Fort Collins, 80523, USA

<sup>d</sup> Atmospheric and Oceanic Sciences Program, Princeton University, Princeton, 08544, USA

<sup>e</sup> Computational Sciences and Engineering Division and Climate Change Science Institute, Oak Ridge National Laboratory, Oak Ridge, 37830, USA

Received 22 January 2021; revised 24 June 2021; accepted 1 July 2021

Available online 19 July 2021

## Abstract

Understanding historical wildfire variations and their environmental driving mechanisms is key to predicting and mitigating wildfires. However, current knowledge of climatic responses and regional contributions to the interannual variability (IAV) of global burned area remains limited. Using recent satellite-derived wildfire products and simulations from version v1.0 of the land component of the U.S. Department of Energy's Energy Exascale Earth System Model (E3SM land model [ELM] v1) driven by three different climate forcings, we investigated the burned area IAV and its climatic sensitivity globally and across nine biomes from 1997 to 2018. We found that 1) the ELM simulations generally agreed with the satellite observations in terms of the burned area IAV magnitudes, regional contributions, and covariations with climate factors, confirming the robustness of the ELM to the usage of different climate forcing sources; 2) tropical savannas, tropical forests, and semi-arid grasslands near deserts were primary contributors to the global burned area IAV, collectively accounting for 71.7%–99.7% of the global wildfire IAV estimated by both the satellite observations and ELM simulations; 3) precipitation was a major fire suppressing factor and dominated the global and regional burned area IAVs, and temperature and shortwave solar radiation were mostly positively related with burned area IAVs; and 4) noticeable local discrepancies between the ELM and remote-sensing results occurred in semi-arid grasslands, croplands, boreal forests, and wetlands, likely caused by uncertainties in the current ELM fire scheme and the imperfectly derived satellite observations. Our findings revealed the spatiotemporal diversity of wildfire variations, regional contributions and climatic responses, and provided new metrics for wildfire modeling, facilitating the wildfire prediction and management.

**Keywords:** Wildfire; Burned area; Climatic sensitivity; E3SM land model; Global fire emission database

## 1. Introduction

An average of 400 million  $\text{hm}^2$ , or about 3% of the global land area, is burned annually by wildfires (Chuvienco et al., 2016; Giglio et al., 2013). Such widespread wildfires have direct impacts on the global carbon cycle, ecosystem dynamics,

atmospheric chemistry, and human society sustainability (Bowman et al., 2009; Page et al., 2002; Shakesby, 2011). In the context of climate warming and increased human activities, fire regimes have shifted dramatically in many regions, such as the Mediterranean area (Mouillot et al., 2002), boreal area (Kasischke et al., 1995), Australia (Cary and Banks, 2000), and the western USA (Abatzoglou and Williams, 2016; Flannigan et al., 2009; McKenzie and Littell, 2017). The interannual variability (IAV) of wildfires is a key fire characteristic that affects the terrestrial carbon cycle and atmospheric composition (e.g.,  $\text{CO}_2$  and aerosol concentrations) (Patra et al., 2005).

\* Corresponding author. 1 Bethel Valley Rd, Oak Ridge, TN, 37830, USA.  
E-mail address: [maoj@ornl.gov](mailto:maoj@ornl.gov) (MAO J.).

Peer review under responsibility of National Climate Center (China Meteorological Administration).

High year-to-year wildfire changes also make wildfire analysis and simulation challenging (Beck et al., 2002), adding complexity to relevant policy decisions, planning, and execution (Monzón-Alvarado et al., 2014; van Wilgen, 2009). Improving the understanding of wildfire IAV and associated environmental determinants is critical for wildfire prediction and management, facilitating the mitigation of adverse wildfire effects on human health and ecological stability.

Our knowledge of global wildfire IAV and its climatic drivers remains limited. Although a number of studies, using observational or modeling approaches, have explored the relationships between wildfire IAV and climate at regional scales (e.g., Africa, Mediterranean area, Siberia), the wildfire-climate relationships are still poorly characterized at the global scale (Abatzoglou et al., 2018; Archibald et al., 2010; Goss et al., 2020; Jolly et al., 2015; Urbietta et al., 2015). Although possible impacts of major climatic factors (e.g., temperature, precipitation, solar radiation) on wildfire IAV have been examined, their relative contributions and corresponding uncertainties still need to be quantified (Crockett and Leroy Westerling, 2018; Fasullo et al., 2018; Holden et al., 2007; Lafon and Quiring, 2012; Wei et al., 2020). Satellite-retrieved wildfire products (e.g., burned area) provide unique opportunities to investigate wildfire dynamics and their climatic determinants across different scales. However, remote-sensing wildfire observations are produced only for recent time periods (e.g., starting from 1997), and the data quality is subject to sensor aging, cloud and smoke disturbances, and the performance of detection algorithms (Giglio et al., 2016; Randerson et al., 2012). Moreover, satellite wildfire datasets are not derived based on physical mechanisms and therefore cannot be directly used to predict future fire behaviors. Process-oriented fire models, designed at different complexity levels, have been developed to simulate historical and future wildfires responding to prescribed or prognostic environmental conditions (Li et al., 2012; 2013; Rabin et al., 2017; Thonicke et al., 2010). However, it is necessary to comprehensively benchmark existing wildfire models against various sources of satellite and ground observations (Korontzi et al., 2006; Ramankutty et al., 2008). Hence, the combined use of remote-sensing and model results would integrate the strengths of both approaches and improve the understanding and mechanistic modeling of global wildfire IAV.

Having a comprehensive understanding of global wildfire IAV and its major climatic drivers would enhance the capability of wildfire prediction and preparedness of wildfire risk management. To achieve this overarching goal, in this study, we focused on addressing the following questions: 1) What were the spatial and temporal structures of global burned area IAV for the 1997–2018 period? 2) What were the biome-level regional contributions to global wildfire IAV? 3) What were the covariations between wildfire IAV and main climate factors? 4) How different were the IAV estimations between ELM and remote-sensing wildfire products? We assessed these changes and performed relevant intercomparisons using different global satellite-based burned area products and offline simulations from version 1.0 of the land component of the U.S. Department of Energy's Energy Exascale Earth System Model (E3SM land model [ELM] v1).

## 2. Data and methodologies

### 2.1. Data

#### 2.1.1. Remote-sensing wildfire products

Two satellite-based wildfire datasets were applied, including the burned area fraction of the Global Fire Emission Database (GFED) version 4.1s (Randerson et al., 2015) and the FireCCI version 5.1 from the European Space Agency Climate Change Initiative (CCI) project (Chuvieco et al., 2018; Lizundia-Loiola et al., 2020). The monthly GFED4.1s burned area fraction spanning from 1997 to 2016 with a spatial resolution of  $0.25^\circ \times 0.25^\circ$  was derived from a combination of multiple data sources that include images from the Visible and Infrared Scanner on the Tropical Rainfall Measuring Mission satellite, multi-channel images of the Along Track Scanning Radiometers on the European Space Agency's Earth-observing satellite, and burned area and thermal products from the Moderate Resolution Imaging Spectroradiometer (MODIS) on the Terra and Aqua satellites (Giglio et al., 2013). When compared with GFED version 4, the version 4.1s dataset accounts for small fires. The FireCCI5.1 burned area dataset was generated from 250 m resolution MODIS red and near-infrared reflectance information, with a combination of thermal anomaly data from the MODIS active fires product (Chuvieco et al., 2018; Giglio et al., 2016; Lizundia-Loiola et al., 2020) and has monthly and biweekly temporal resolutions from 2001 to present.

Both GFED4.1s and FireCCI5.1 dataset were aggregated to  $0.5^\circ \times 0.5^\circ$  resolution with yearly intervals covering 1997–2016 and 2001–2018, respectively. Because GFED4.1s provides a burned area fraction in each grid, we multiplied it by the land area of each  $0.5^\circ$  grid to derive actual burned areas. Only pixels with annual mean Normalized Difference Vegetation Index greater than 0.125 were considered to ensure available combustible biomass and spatial consistency among different data sources (Pinzon and Tucker, 2014). A similar vegetation classification scheme like (Ahlström et al., 2015) was adopted and includes tropical rainforests (TRFs), temperate forests (TEFs), boreal forests (BFs), tropical savannahs (TRS), temperate grasslands and shrublands (TGRSSs), semi-arid grasslands (SAGs), tundra (TUD), croplands (CRPs), and wetlands (WETs) (Fig. A1).

#### 2.1.2. ELM wildfire simulations

Built on the Community Land Model Version 4.5 (CLM4.5), the ELM embeds the CLM-Li fire scheme (Li et al., 2012, 2013) as the default fire component. CLM-Li contains four sub-modules: process-based non-peat fires, empirical agricultural fires, deforestation fires, and peat fires. The simulated fire-burned area, mainly the non-peat burned area, is estimated as a function of fire counts and an average fire spread area driven by ignition sources, fuel load, fuel combustibility, and anthropogenic suppression processes. For this study, the global burned area simulations were produced by three offline ELM experiments driven by different climate forcings, including CRUNCEP version 8 (1901–2016), GSWP version 2 (1901–2014), and PRINCETON (1901–2012) (van Den Hurk

et al., 2016). Accordingly, these three historical simulations at 0.5° spatial resolution were denoted as ELM-CRU, ELM-GSWP, and ELM-PRIN, respectively. A more detailed description of the experimental setup and driver information for ELM historical transient runs can be found in Chen et al. (2020), Forbes et al. (2018, 2019), and Haarsma et al. (2016).

## 2.2. Methodologies

### 2.2.1. IAV

Similar to previous studies (Anderegg et al., 2015; Fu et al., 2017; Piao et al., 2020), we defined the detrended annual anomalies of wildfire or climate variables as their interannual variability (IAV). Specifically, the IAV of variable  $Y$  is denoted as:

$$I = Y - \hat{Y} \quad (1)$$

where  $Y$  is the original time series and  $\hat{Y}$  is the fitting line from a least squares regression.

The magnitude of IAV is characterized using the coefficient variations (CV) (Chuvieco et al., 2021):

$$CV = \frac{\sigma}{\mu}, \quad (2)$$

where  $\sigma$  and  $\mu$  stand for the standard deviation and mean.

### 2.2.2. Regional contribution index

An IAV contribution partitioning index (Ahlström et al., 2015) was used to calculate the contribution of each biome type to global burned area IAV. The contribution index  $f_j$  is defined as

$$f_j = \frac{\sum_t \frac{b_{jt}|B_t|}{B_t}}{\sum_t |B_t|} \quad (3)$$

where  $b_{jt}$  is the detrended burned area for biome region  $j$  in year  $t$  and  $B_t$  is the detrended global burned area, where  $B_t = \sum_j b_{jt}$ . This definition implies  $\sum_j f_j = 1$ . The resulting index  $f_j$  represents region  $j$ 's contribution to global variation. A region with higher index means it contributes more to the global variation, and a negative index dampens global variation. Each regional contribution index was multiplied by 100 to convert fractions to percentages.

Partial correlation analysis was employed at grid, biome, and global scales to explore sensitivities of burned area IAV to various climate factors (i.e., temperature, precipitation, and solar downward radiation). Long-term linear trends were removed before conducting partial correlations.

## 3. Results

The ELM global burned area IAV ranged from  $-44.0$  to  $57.6$   $\text{Mhm}^2$  (e.g.,  $-36.7$ – $36.8$   $\text{Mhm}^2$  for ELM-CRU,  $-44.0$ – $57.6$

$\text{Mhm}^2$  for ELM-GSWP, and  $-34.6$ – $43.1$   $\text{Mhm}^2$  for ELM-PRIN), generally consistent with satellite-derived results, especially with the GFED4.1s (i.e.,  $-45.2$ – $42.2$   $\text{Mhm}^2$  for GFED4.1s and  $-93.0$ – $48.0$   $\text{Mhm}^2$  for the FireCCI5.1) (Fig. 1; Table A1). Global wildfire IAV magnitudes from different ELM simulations, represented by CV, also agreed closely with that of satellite-derived results in the period of 1997–2012 (i.e., 0.1 for ELM-CRU, 0.1 for ELM-GSWP, 0.1 for ELM-PRIN, and 0.1 for GFED4.1s). The IAV of FireCCI5.1 global burned area was abnormally low in 2001, which was mainly contributed by the low IAV values from the TRF and TRS biomes (Fig. A2a and d). Such underestimation was likely caused by the absence of MODIS Aqua Hotspots data between 2001/01 and 2002/07 (Chuvieco et al., 2018; Lizundia-Loiola et al., 2020). Considering the relatively short temporal overlap of FireCCI5.1 with other datasets (starting from 2001), GFED4.1s will thus hereafter be primarily used to compare with the ELM simulations.

Geographically, a relatively high IAV variation of GFED4.1s occurred mainly in the boreal area and semi-arid region (e.g., Australia), while tropical and subtropical regions showed relatively low fire variations (Fig. 2a). The weakest wildfire variations existed in African subtropical savannah systems and were consistent with previous studies (Archibald et al., 2013; Chuvieco et al., 2008). Such a remote-sensing-derived spatial pattern was generally reproduced by the ELM simulations, especially the ELM-GSWP and ELM-PRIN, which were mostly consistent with one another (Fig. 2b–d). However, some regional discrepancies between the ELM and GFED4.1s variation magnitudes were noteworthy. For example, the ELM underestimated the IAV magnitudes in the boreal area, especially the ELM-CRU, and the ELM overestimated the IAV over Africa.

The ELM simulations driven by different climate forcings consistently produced the highest IAV variation in the Boreal Forests (BF) ( $0.5 \pm 0.2$ ), the second highest variation in the Tundra (TUD) ( $0.4 \pm 0.1$ ), and the lowest variation in the temperate grasslands and shrubland (TGRS) ( $0.1 \pm 0.0$ ) (Fig. 3a). GFED4.1s showed the highest wildfire variation in the TUD (1.5), followed by BF (1.1), while the Tropical Savannas (TRS) had the lowest variation (0.1). For the regional

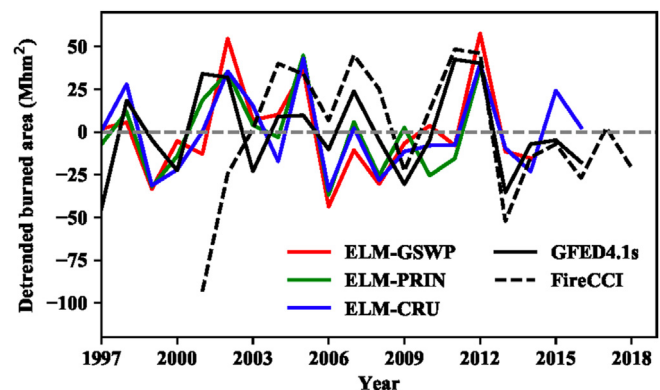


Fig. 1. Global burned area IAVs from 1997 to 2018 of simulation results.

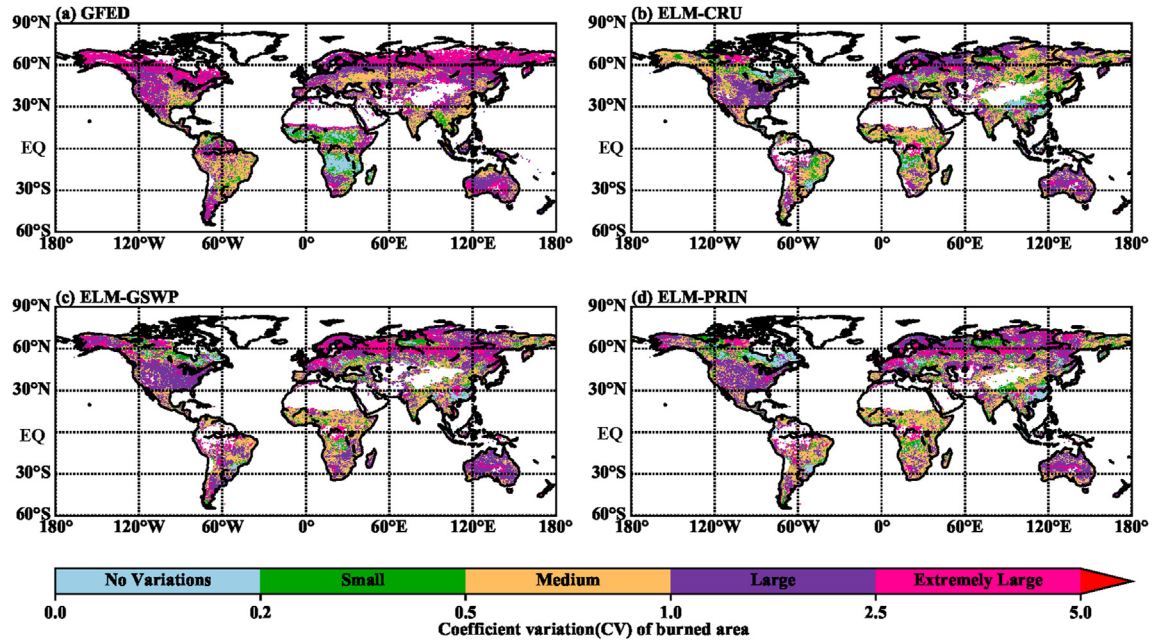


Fig. 2. Spatial distribution of coefficient variation of burned area for (a) GFED, (b) the ELM-CRU, (c) the ELM-GSWP, and (d) the ELM-PRIN for 1997–2012.

contribution, both types of products estimated that TRSs contributed most to the global IAV (58.0% for ELM-CRU, 42.0% for ELM-GSWP, 58.3% for ELM-PRIN, and 58.4% for GFED4.1s). The second leading contribution was from TRFs for the ELM simulations (14.7% for ELM-CRU, 22.0% for ELM-GSWP, and 18.2% for ELM-PRIN), and from SAGs (31.8%) for the GFED retrieval.

Both GFED4.1s and ELM simulations showed that the burned area IAV correlated positively with temperature and shortwave radiation but correlated negatively with precipitation for most of the globe (Fig. 4). One noticeable exception, however, existed in northern Australia, where the GFED wildfire generally showed negative temperature responses while ELM wildfire simulations demonstrated slightly positive temperature responses (Fig. 4a–b, Figs. A4 and A6). In this area, high temperature and associated droughts tend to limit the vegetation growth, resulting in less available fuel for burning (Bradstock, 2010; Sun et al., 2019; Madani et al., 2020). But detailed climatic and anthropogenic driving mechanisms (e.g., the traditional Indigenous fire management) underlying the wildfire IAV in this local region are still uncertain and require further investigation (Bowman et al., 2020). Compared with the GFED4.1s, the ELM simulated burned area IAVs were more sensitive to precipitation, especially in North America and northern Eurasia (Fig. 4d), and were more sensitive to temperature and shortwave radiation, mainly in North America (Fig. 4a, b, e, and f). Different sources of climate forcings had minor impacts on their correlations with burned area IAV for either wildfire product (Fig. 4, and Fig. A4). Additionally, the spatial patterns for climate sensitivities of ELM wildfire IAVs were broadly consistent among the simulations driven by different climate forcings (Fig. 4, and Fig. A4).

Regional summaries of both GFED4.1s and ELM sensitivity results, shown in Fig. 5, confirmed positive responses of burned area IAV to temperature and shortwave radiation but negative responses to precipitation across the globe and most biome regions. Moreover, precipitation mainly controlled the burned area IAV, especially for the three ELM simulations. Major response differences between the ELM and observations were found in the BF, SAG, and WET biomes in terms of the sensitivity magnitude, sign, or both.

#### 4. Discussion

Using the latest satellite and ELM-simulated wildfire products, we investigated global and regional wildfire IAVs and their climatic sensitivities. The findings of regional contributions to the global burned area IAV and the impacts of major climatic factors on the changes of burned area IAVs are generally consistent with previous wildfire assessments (Randerson et al., 2012; van der Werf et al., 2006; 2008a; 2008b; Yin et al., 2016). Next, we will discuss the burned area IAV and its underlying mechanisms for each biome, starting with the TRS because of its largest contribution to global IAV.

TRSs, featured with high fire intensity but low IAV variation magnitude, were the largest contributor to the global burned area IAV. TRSs, such as the African TRS systems, are characterized by the codominance of C3 woody plants and C4 grasses. During wet seasons or years, grasses prevail and form a dense herbaceous layer, which then dries quickly in dry seasons or years. Such seasonal or interannual variation of grass fuel availability, mainly driven by rainfall patterns, favors biomass combustion all year round and leads to the largest regional contribution to global burned area variation

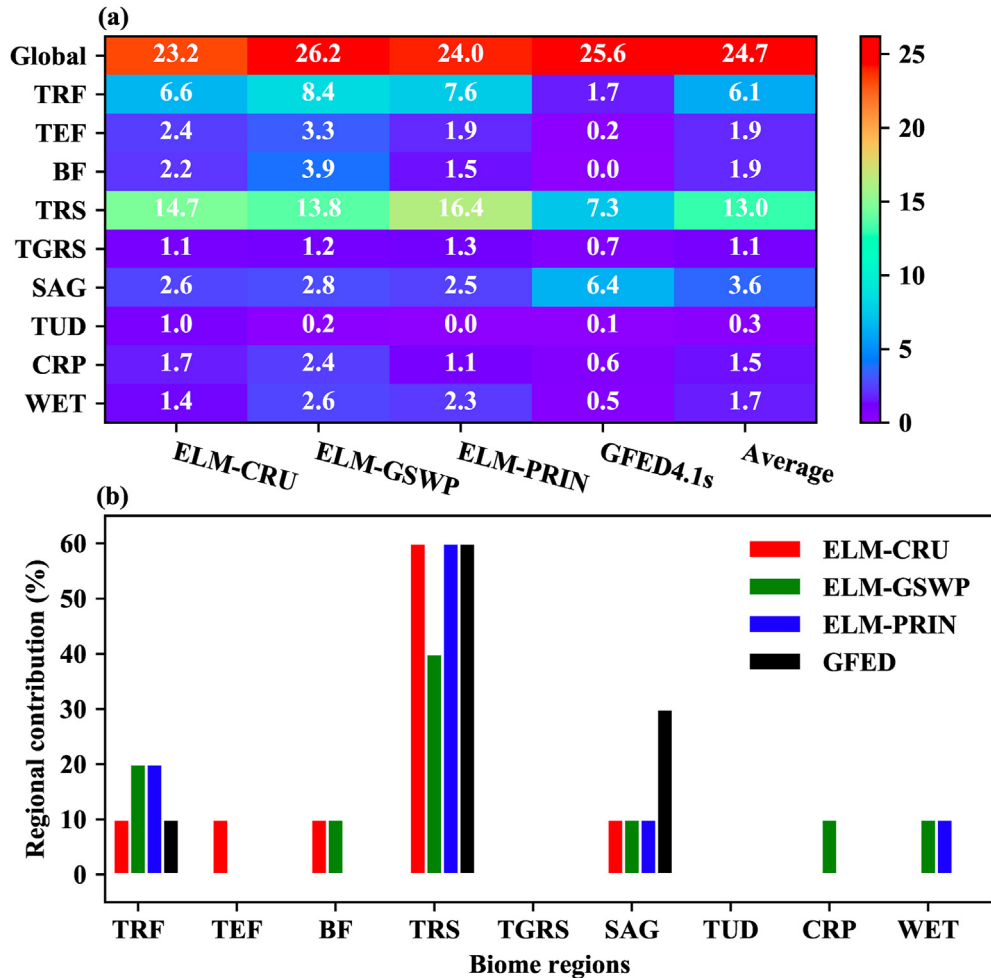


Fig. 3. Global and regional burned area coefficient variation (a); and (b) relative percentages of regional IAV contribution to global burned area IAV from 1997 to 2012 for the tropical rainforest (TRF), temperate forests (TEF), boreal forest (BF), tropical savannah (TRS), temperate grasslands and shrubland (TGRS), semi-arid grassland (SAG), tundra (TUD), cropland (CRP), and wetlands (WET) biomes.

(Archibald et al., 2010; Hao and Liu, 1994; Romero-Ruiz et al., 2010).

Next to TRSs, TRFs also showed a large contribution to the global burned area IAV. These high wildfire numbers of TRFs, especially those in tropical Asia, were likely associated with irregular peatland drainage and deforestation that are partially caused by political and economic incentives (Cochrane, 2001; Laurance and Williamson, 2001; Morton et al., 2006; Murdiyarso et al., 2004; Shea et al., 1996). The draining of peatlands and consequently lowered water-table levels would not only induce a higher peat decomposition rate but also make peat areas more fire-prone (Hirano et al., 2014; Konecny et al., 2016; Miettinen et al., 2012). Tropical deforestation, forest thinning, or removing the forest canopy would allow greater insolation to the soil surface, resulting in a more flammable environment with dryer fuel, higher air temperature and wind speed, lower relative humidity, and less precipitation (Christopher and Kauffman, 1990; Hoffmann, 2003; Xu et al., 2020).

The global SAG biome, covering the desert grasslands, was found to make a large contribution to the global burned area

IAV, especially for the GFED4.1s (Fig. 3b). Over recent decades, more mega-fires have occurred in its corresponding geographical locations, such as those in western Australia (Haydon et al., 2000) and the western USA (Abatzoglou and Kolden, 2011). Such wildfire increases in SAGs were likely linked to the rain-related growth of domestic grasses and expansion of plant invasions such as the red brome and cheatgrass invasion in North America, gamba grass and buffelgrass in northern and central Australia (Clarke et al., 2005), and buffelgrass invasion in the southwestern USA (Mack, 1981; Marshall et al., 2012; Setterfield et al., 2010). The increase of exotic grasses and associated loss of native shrubbery or woody vegetation significantly changes fuel characteristics, such as a growing fuel continuity and fuel load (Brooks et al., 2004; Horn et al., 2015; Horn and St. Clair, 2017; McLaughlin and Bowers, 1982; Wright, 1980). For example, buffelgrass in Australia, is highly drought-tolerant and thus more flammable than domestic grasses by providing more biomass and higher spatial connectivity (Clarke et al., 2005). No matter what types of grass exist in the SAG, precipitation was widely reported to have a positive correlation with fire events since it dominants

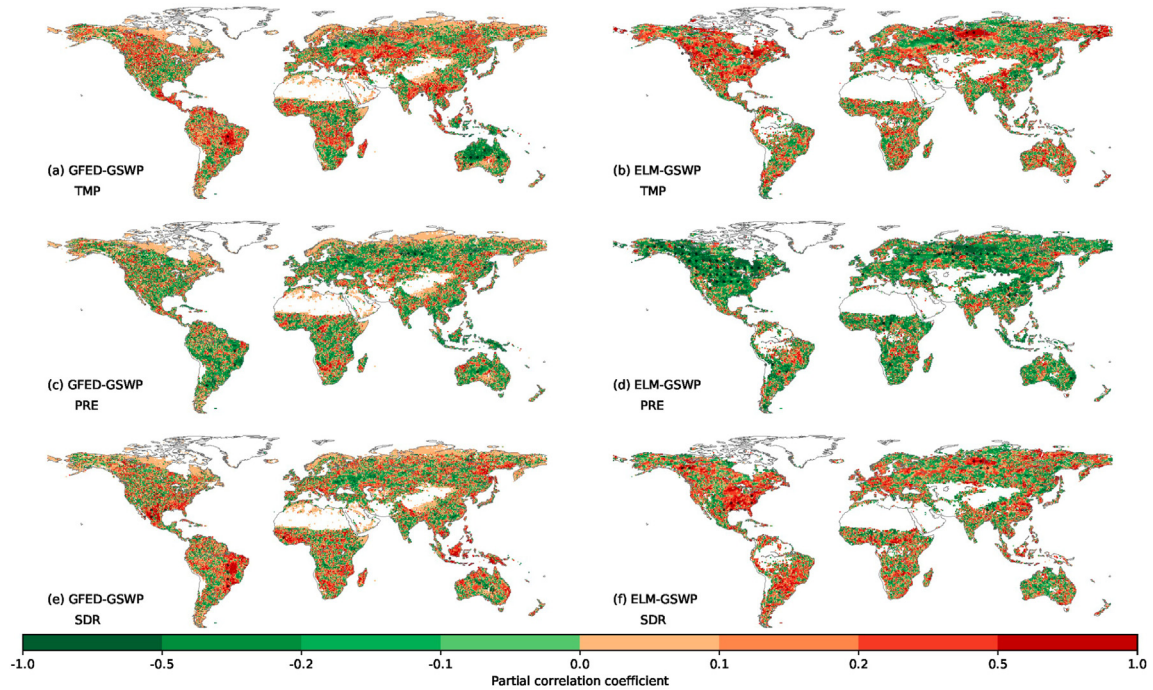


Fig. 4. Spatial distributions of partial correlation coefficients between burned area IAVs and different climate factors from 1997 to 2012 (a, c, e) partial correlations between the GFED4.1s burned area IAV and each climate forcing of GSWP; and (b, d, f) partial correlations between the ELM burned area IAV and each climate forcing of GSWP (Pixels with statistical significance ( $p < 0.1$ ) are black dotted; TMP, PRE, and SDR represent temperature, precipitation, and solar downward radiation, respectively).

grass growth and provides fuel for combustions in the dry season (Bradstock, 2010).

The wildfire IAV showed vast spatial variation, being dominated or co-dominated by different climatic factors over different geographical regions (Figs. 4 and 5 and Fig. A5). In accordance with previous results, temperature was identified to mostly determine the wildfire IAVs in high-latitude areas with

positive partial correlations. Local warming could increase tree mortality in those areas, enhance evapotranspiration, lower relative humidity, and thus lead to more flammable biomass fuel and drier weather, favoring the ignition and spreading of wildfires (Allen et al., 2010; Anderegg et al., 2013; Breshears et al., 2005). Both the ELM and satellite results roughly agreed that precipitation was the major

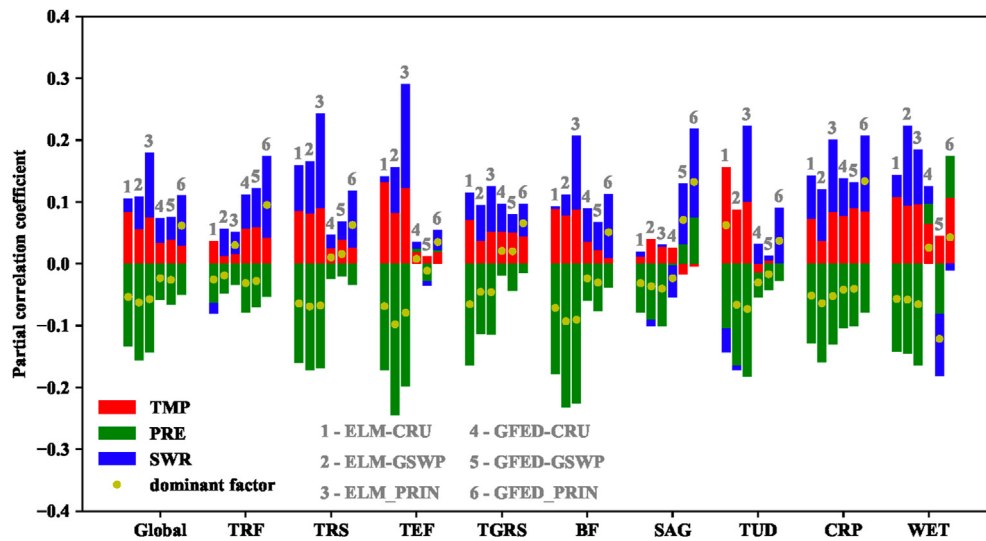


Fig. 5. Summaries of partial correlations between burned area IAV and climate factors for the globe (Global), tropical rainforest (TRF), tropical savannah (TRS), temperate forests (TEF), temperate grasslands and shrubland (TGRS), boreal forest (BF), semi-arid grassland (SAG), tundra (TUD), cropland (CRP), and wetlands (WET) (Visible length of each bar stands for the magnitude of partial correlation; the dominant climate factor is the one with the highest absolute value of partial correlation).

suppressing factor for global wildfire IAVs (Fig. 4c, d, Fig. A4b, e, h, k, and Fig. 5). Precipitation patterns have been widely confirmed to govern wildfire variations by changing the fuel load and fuel moisture (Andela and van der Werf, 2014; Archibald et al., 2009). For example, the burned area variation in TEFs of the western USA was strongly associated with the vegetation condition and soil wetness, which were directly or indirectly affected by the summer precipitation changes (Holden et al., 2018). In TGRSs, many studies have revealed that precipitation stimulates plant photosynthesis, favors biomass accumulation, and thus may increase fire probability (Pilliod et al., 2017; Song et al., 2016; Vargas et al., 2012). However, the ignition of wildfires in TGRSs also relies on the alternating pattern of wet and dry years for a flammable environment with enough dry fuel and fuel continuity. Thus, for this research, the identified annual constraining effects of precipitation on TGRS wildfire variation (Fig. 5) were likely more controlled by the precipitation-induced high fuel moisture than the precedented precipitation-stimulated high fuel availability.

This study demonstrates that the ELM generally captured the IAV variation magnitudes of remote-sensing burned areas at the global scale (Fig. 2). Furthermore, ELM simulations driven by different climate forcings (i.e., the ELM-CRU, ELM-GSWP, and ELM-PRIN) produced similar sensitivities of burned area IAVs to climate factors, reflecting the model's steady performance and robustness in simulating the wildfire-climate feedback (Fig. 4 and Fig. A4). However, when comparing the burned area IAVs derived from satellite observations and model simulations, we also found discrepancies in the SAG biome around deserts for its IAV variation magnitude, global contribution, and responses to climate factors. Moderate inconsistencies were also identified in BFs, CRPs, and WETs, and the ELM simulations tended to be more sensitive to climatic factors than GFED4.1s, especially in North America. Such disparities between the two products could be caused for various reasons such as imperfect modeling representations and defective satellite-extracted observations. Because the interactions between burned areas and their environmental drivers are complex and nonlinear, the statistical assumption of the climate-fire relationship as a linear system in this study may lead to considerable uncertainties (Archibald et al., 2010; Hantson et al., 2016; Kloster and Lasslop, 2017). Although in the current ELM-Li fire scheme, population density and gross domestic product are used to characterize human impacts on wildfire dynamics, the monotonically increasing or decreasing expressions of these two factors may induce performance degradation. The default fire scheme also ignores anthropogenic impacts on the seasonality of wildfires, especially over agricultural regions and heavily deforested areas. In CRPs where rice is grown, for example, the fire season timing and the number of peak months may vary significantly because of different agricultural cultivating modes. The oversimplified representation of land use and land cover change in the ELM model and possible classification errors, especially between peatland and WETs, also lead to a modeling limitation of the time-varying burned

areas. Additionally, the current fire model assumes that fuel load, which is mainly the above-ground biomass, is constant within one particular year and does not change over seasons with the climates, human activities, and even wildfire feedback. This could be a major reason why the model underestimated burned area IAVs in SAG areas, where wildfire occurrences largely depend on the seasonal fuel accumulation, especially during wet seasons (Gremer et al., 2015; Rao and Allen, 2010). The IAV magnitudes in BFs and TUDs were much different between simulations and satellite observations (Fig. 3a). Peatland covers about 25%–30% of the BF region, and forested peatland is vulnerable to wildfires (Gorham, 1991; Gremer et al., 2015; Wieder and Vitt, 2006). Although the parameterization of ELM peatland fires may be further improved by using more accurate peat maps and considering time-depending burning depth, ELM produced similar wildfire IAVs to those from the satellite-derived FireCCI5.1, while GFED4.1s yielded low IAVs over the BFs and TUDs (Fig. A2c, and g). Burned areas in the GFED4.1s were derived by an algorithm that applied a burn-sensitive vegetation index with a threshold of active fires. Smoldering peatland wildfires could be too difficult to detect because of the mixture of peatlands with upland BFs, which may have resulted in the underestimated wildfire IAVs for GFED4.1s.

## 5. Conclusions

Using satellite-derived wildfire products and process-oriented ELM simulations, this study explored the spatio-temporal dynamics of burned area IAVs and their possible responses to major climatic factors. The wildfire activities in tropical savannas, tropical forests, and SAGs around deserts were found to dominate the global burned area IAV and were mainly associated with the precipitation variations, especially for the ELM outputs. Both temperature and downward shortwave radiation positively modulated the burned area IAV, whereas precipitation showed significant suppressing effects across most regions for both types of fire products. Satellite and ELM IAVs and their covariations with climate factors were mostly consistent at the global scale, and the ELM simulations were robust even when driven by different climate inputs. However, some discrepancies regarding sign, magnitude, or both were identified in SAG, BF, TUD, CRP, and WET areas. Both the ELM uncertainties and observational biases in the satellite products may lead to such discrepancies. A need exists to improve the ELM fire processes and capture the effects of different land surface conditions, climate change, and human activities, especially for the CRP, SAG and peatland fires. Such detailed global quantification of wildfire IAVs and associated driving mechanisms offers important insights into the wildfire prediction, management, and sustainable maintenance, especially across fire-prone regions.

## Declaration of competing interest

The authors declare no conflict of interest.

## Acknowledgments

This work is supported by the Terrestrial Ecosystem Science Scientific Focus Area project and the Reducing Uncertainties in Biogeochemical Interactions through Synthesis and Computing Scientific Focus Area project funded by the U.S. Department of Energy, Office of Science, Office of Biological and Environmental Research. The authors also acknowledge Dr. Daniel Ricciuto for his contribution to the global ELM simulations. Oak Ridge National Laboratory is supported by the Office of Science of the U.S. Department of Energy under Contract No. DE-AC05-00OR22725.

## Appendix A. Supplementary data

Supplementary data to this article can be found online at <https://doi.org/10.1016/j.accre.2021.07.001>.

## References

- Abatzoglou, J.T., Kolden, C.A., 2011. Climate change in Western U.S. deserts: potential for increased wildfire and invasive annual grasses. *Rangel. Ecol. Manag.* 64, 471–478. <https://doi.org/10.2111/REM-D-09-00151.1>.
- Abatzoglou, J.T., Williams, A.P., 2016. Impact of anthropogenic climate change on wildfire across western U.S. forests. *Proc. Natl. Acad. Sci. U. S. A.* 113, 11770–11775. <https://doi.org/10.1073/pnas.1607171113>.
- Abatzoglou, J.T., Williams, A.P., Boschetti, L., et al., 2018. Global patterns of interannual climate-fire relationships. *Global Change Biol.* 24, 5164–5175. <https://doi.org/10.1111/gcb.14405>.
- Ahlström, A., Raupach, M.R., Schurgers, G., et al., 2015. The dominant role of semi-arid ecosystems in the trend and variability of the land CO<sub>2</sub> sink. *Science* 120, 895–899. <https://doi.org/10.1002/2015JA021022>.
- Allen, C.D., Macalady, A.K., Chenhoumi, H., et al., 2010. A global overview of drought and heat-induced tree mortality reveals emerging climate change risks for forests. *For. Ecol. Manag.* 259, 660–684. <https://doi.org/10.1016/j.foreco.2009.09.001>.
- Andela, N., van der Werf, G.R., 2014. Recent trends in African fires driven by cropland expansion and El Niño to la Niña transition. *Nat. Clim. Change* 4, 791–795. <https://doi.org/10.1038/nclimate2313>.
- Anderegg, W.R.L., Kane, J.M., Anderegg, L.D.L., 2013. Consequences of widespread tree mortality triggered by drought and temperature stress. *Nat. Clim. Change* 3, 30–36. <https://doi.org/10.1038/nclimate1635>.
- Anderegg, W.R.L., Hicke, J.A., Fisher, R.A., et al., 2015. Tree mortality from drought, insects, and their interactions in a changing climate. *New Phytol.* 208, 674–683.
- Archibald, S., Roy, D.P., van Wilgen, B.W., et al., 2009. What limits fire? An examination of drivers of burnt area in Southern Africa. *Global Change Biol.* 15, 613–630. <https://doi.org/10.1111/j.1365-2486.2008.01754.x>.
- Archibald, S., Nickless, A., Govender, N., et al., 2010. Climate and the inter-annual variability of fire in southern Africa: a meta-analysis using long-term field data and satellite-derived burnt area data. *Global Ecol. Biogeogr.* 19, 794–809. <https://doi.org/10.1111/j.1466-8238.2010.00568.x>.
- Archibald, S., Lehmann, C.E.R., Gómez-Dans, J.L., et al., 2013. Defining pyromes and global syndromes of fire regimes. *Proc. Natl. Acad. Sci. Unit. States Am.* 110, 6442–6447.
- Beck, J.A., Alexander, M.E., Harvey, S.D., et al., 2002. Forecasting diurnal variations in fire intensity to enhance wildland firefighter safety. *Int. J. Wildland Fire* 11, 173–182. <https://doi.org/10.1071/wf02002>.
- Bowman, D.M.J.S., Balch, J.K., Artaxo, P., et al., 2009. Fire in the earth system. *Science* 324, 481–484. <https://doi.org/10.1126/science.1163886>.
- Bowman, D.M.J.S., Kolden, C.A., Abatzoglou, J.T., et al., 2020. Vegetation fires in the anthropocene. *Nat Rev Earth Environ* 1, 500–515.
- Bradstock, R.A., 2010. A biogeographic model of fire regimes in Australia: current and future implications. *Global Ecol. Biogeogr.* 19, 145–158.
- Breshears, D.D., Cobb, N.S., Rich, P.M., et al., 2005. Regional vegetation die-off in response to global-change-type drought. *Proc. Natl. Acad. Sci. U. S. A.* 102, 15144–15148. <https://doi.org/10.1073/pnas.0505734102>.
- Brooks, M.L., D'Antonio, C.M., Richardson, D.M., et al., 2004. Effects of invasive alien plants on fire regimes. *Bioscience* 54, 677–688. [https://doi.org/10.1641/0006-3568\(2004\)054\[0677:EOIAP0\]2.0.CO;2](https://doi.org/10.1641/0006-3568(2004)054[0677:EOIAP0]2.0.CO;2).
- Cary, G.J., Banks, J.C.G., 2000. Fire regime sensitivity to global climate change: an Australian perspective. In: Innes, J.L., Beniston, M., Verstraete, M.M. (Eds.), *Biomass Burning and Its Inter-relationships with the Climate System*. Springer, Dordrecht, pp. 233–246. [https://doi.org/10.1007/0-306-47959-1\\_13](https://doi.org/10.1007/0-306-47959-1_13).
- Chen, A., Tang, R., Mao, J., et al., 2020. Spatiotemporal dynamics of ecosystem fires and biomass burning-induced carbon emissions in China over the past two decades. *Geogr. Sustain.* 1, 47–58. <https://doi.org/10.1016/j.geosus.2020.03.002>.
- Christopher, U., Kauffman, J.B., 1990. Deforestation, fire susceptibility, and potential tree responses to fire in the Eastern Amazon. *Ecology* 71, 437–449.
- Chuvieco, E., Giglio, L., Justice, C., 2008. Global characterization of fire activity: toward defining fire regimes from Earth observation data. *Global Change Biol.* 14, 1488–1502. <https://doi.org/10.1111/j.1365-2486.2008.01585.x>.
- Chuvieco, E., Yue, C., Heil, A., et al., 2016. A new global burned area product for climate assessment of fire impacts. *Global Ecol. Biogeogr.* 25, 619–629. <https://doi.org/10.1111/geb.12440>.
- Chuvieco, E., Lizundia-Loiola, J., Lucrecia Pettinari, M., et al., 2018. Generation and analysis of a new global burned area product based on MODIS 250 m reflectance bands and thermal anomalies. *Earth Syst. Sci. Data* 10, 2015–2031. <https://doi.org/10.5194/essd-10-2015-2018>.
- Chuvieco, E., Pettinari, M.L., Koutsias, N., et al., 2021. Human and climate drivers of global biomass burning variability. *Sci. Total Environ.* 779, 146361.
- Clarke, P.J., Latz, P.K., Albrecht, D.E., 2005. Long-term changes in semi-arid vegetation: invasion of an exotic perennial grass has larger effects than rainfall variability. *J. Veg. Sci.* 16, 237–248.
- Cochrane, M.A., 2001. Synergistic interactions between habitat fragmentation and fire in evergreen tropical forests. *Conserv. Biol.* 15, 1515–1521. <https://doi.org/10.1046/j.1523-1739.2001.01091.x>.
- Crockett, J.L., Leroy Westerling, A., 2018. Greater temperature and precipitation extremes intensify Western U.S. droughts, wildfire severity, and sierra Nevada tree mortality. *J. Clim.* 31, 341–354. <https://doi.org/10.1175/JCLI-D-17-0254.1>.
- Fasullo, J.T., Otto-Bliesner, B.L., Stevenson, S., 2018. ENSO's changing influence on temperature, precipitation, and wildfire in a warming climate. *Geophys. Res. Lett.* 45, 9216–9225. <https://doi.org/10.1029/2018GL079022>.
- Flannigan, M., Stocks, B., Turetsky, M., et al., 2009. Impacts of climate change on fire activity and fire management in the circumboreal forest. *Global Change Biol.* 15, 549–560. <https://doi.org/10.1111/j.1365-2486.2008.01660.x>.
- Forbes, W.L., Mao, J., Jin, M., et al., 2018. Contribution of environmental forcings to U.S. runoff changes for the period 1950–2010. *Environ. Res. Lett.* 13, 054023. <https://doi.org/10.1088/1748-9326/aabb41>.
- Forbes, W.L., Mao, J., Ricciuto, D.M., et al., 2019. Streamflow in the Columbia River Basin: quantifying changes over the period 1951–2008 and determining the drivers of those changes. *Water Resour. Res.* 55, 6640–6652. <https://doi.org/10.1029/2018wr024256>.
- Fu, Z., Dong, J., Zhou, Y., et al., 2017. Long term trend and interannual variability of land carbon uptake: the attribution and processes. *Environ. Res. Lett.* 12. <https://doi.org/10.1088/1748-9326/aa5685>.
- Giglio, L., Schroeder, W., Justice, C.O., 2016. The collection 6 MODIS active fire detection algorithm and fire products. *Remote Sens. Environ.* 178, 31–41. <https://doi.org/10.1016/j.rse.2016.02.054>.
- Giglio, L., Randerson, J.T., van der Werf, G.R., 2013. Analysis of daily, monthly, and annual burned area using the fourth-generation global fire emissions database (GFED4). *J. Geophys. Res. Biogeosci.* 118, 317–328. <https://doi.org/10.1002/jgrg.20042>.

- Gorham, E., 1991. Northern peatlands: role in the carbon cycle and probable responses to climatic warming. *Ecol. Appl.* 1, 182–195.
- Goss, M., Swain, D.L., Abatzoglou, J.T., et al., 2020. Climate change is increasing the likelihood of extreme autumn wildfire conditions across California. *Environ. Res. Lett.* 15, 094016 <https://doi.org/10.1088/1748-9326/ab83a7>.
- Gremer, J.R., Bradford, J.B., Munson, S.M., et al., 2015. Desert grassland responses to climate and soil moisture suggest divergent vulnerabilities across the southwestern United States. *Global Change Biol.* 21, 4049–4062. <https://doi.org/10.1111/gcb.13043>.
- Hao, W.M., Liu, M.H., 1994. Spatial and temporal distribution of tropical biomass burning. *Global Biogeochem. Cycles* 8, 495–503. <https://doi.org/10.1029/94GB02086>.
- Haarsma, R.J., Roberts, M.J., Vidale, P.L., et al., 2016. High resolution model intercomparison project (HighResMIP v1.0) for CMIP6. *Geosci. Model Dev. (GMD)* 9, 4185–4208. <https://doi.org/10.5194/gmd-9-4185-2016>.
- Hantson, S., Armeth, A., Harrison, S.P., et al., 2016. The status and challenge of global fire modelling. *Biogeosciences* 13, 3359–3375. <https://doi.org/10.5194/bg-13-3359-2016>.
- Haydon, D.T., Friar, J.K., Pianka, E.R., 2000. Fire-driven dynamic mosaics in the Great Victoria Desert, Australia: I. fire geometry. *Landsc. Ecol.* 15, 373–382.
- Hirano, T., Kusin, K., Limin, S., et al., 2014. Carbon dioxide emissions through oxidative peat decomposition on a burnt tropical peatland. *Global Change Biol.* 20, 555–565. <https://doi.org/10.1111/gcb.12296>.
- Hoffmann, W.A., 2003. Regional feedbacks among fire, climate, and tropical deforestation. *J. Geophys. Res.* 108, 1–11. <https://doi.org/10.1029/2003jd003494>.
- Holden, Z.A., Morgan, P., Crimmins, M.A., et al., 2007. Fire season precipitation variability influences fire extent and severity in a large southwestern wilderness area, United States. *Geophys. Res. Lett.* 34, 1–5. <https://doi.org/10.1029/2007GL030804>.
- Holden, Z.A., Swanson, A., Luce, C.H., et al., 2018. Decreasing fire season precipitation increased recent western U.S. forest wildfire activity. *Proc. Natl. Acad. Sci. U. S. A.* 115, E8349–E8357. <https://doi.org/10.1073/pnas.1802316115>.
- Horn, K.J., St. Clair, S.B., 2017. Wildfire and exotic grass invasion alter plant productivity in response to climate variability in the Mojave Desert. *Landsc. Ecol.* 32, 635–646. <https://doi.org/10.1007/s10980-016-0466-7>.
- Horn, K.J., Wilkinson, J., White, S., et al., 2015. Desert wildfire impacts on plant community function. *Plant Ecol.* 216, 1623–1634. <https://doi.org/10.1007/s11258-015-0546-9>.
- Jolly, W.M., Cochran, M.A., Freeborn, P.H., et al., 2015. Climate-induced variations in global wildfire danger from 1979 to 2013. *Nat. Commun.* 6, 1–11. <https://doi.org/10.1038/ncomms8537>.
- Kasischke, E.S., Christensen, N.L., Stocks, B.J., et al., 1995. Fire, global warming, and the carbon balance of boreal forests. *Ecol. Appl.* 5, 437–451. <https://doi.org/10.2307/1942034>.
- Kloster, S., Lasslop, G., 2017. Historical and future fire occurrence (1850 to 2100) simulated in CMIP5 Earth System Models. *Global Planet. Change* 150, 58–69. <https://doi.org/10.1016/j.gloplacha.2016.12.017>.
- Konecny, K., Ballhorn, U., Navratil, P., et al., 2016. Variable carbon losses from recurrent fires in drained tropical peatlands. *Global Change Biol.* 22, 1469–1480. <https://doi.org/10.1111/gcb.13186>.
- Korontzi, S., McCarty, J., Loboda, T., et al., 2006. Global distribution of agricultural fires in croplands from 3 years of Moderate Resolution Imaging Spectroradiometer (MODIS) data. *Global Biogeochem. Cycles* 20, 1–15. <https://doi.org/10.1029/2005GB002529>.
- Lafon, C.W., Quiring, S.M., 2012. Relationships of fire and precipitation regimes in temperate forests of the eastern United States. *Earth Interact.* 16, 1–15. <https://doi.org/10.1175/2012EJ000442.1>.
- Laurance, W.F., Williamson, G.B., 2001. Positive feedbacks among forest fragmentation, drought, and climate change in the Amazon. *Conserv. Biol.* 15, 1529–1535.
- Li, F., Zeng, X.D., Levis, S., 2012. A process-based fire parameterization of intermediate complexity in a dynamic global vegetation model. *Biogeosciences* 9, 2761–2780. <https://doi.org/10.5194/bg-9-2761-2012>.
- Li, F., Levis, S., Ward, D.S., 2013. Quantifying the role of fire in the Earth system: Part I improved global fire modeling in the Community Earth System Model (CESM1). *Biogeosciences* 10, 2293–2314. <https://doi.org/10.5194/bg-10-2293-2013>.
- Lizundia-Loiola, J., Otón, G., Ramo, R., et al., 2020. A spatio-temporal active-fire clustering approach for global burned area mapping at 250 m from MODIS data. *Remote Sens. Environ.* 236, 111493. <https://doi.org/10.1016/j.rse.2019.111493>.
- Mack, R.N., 1981. Invasion of bromus tectorum L. into western North America: an ecological chronicle. *Agro-Ecosystems* 7, 145–165. [https://doi.org/10.1016/0304-3746\(81\)90027-5](https://doi.org/10.1016/0304-3746(81)90027-5).
- Madani, N., Parazoo, N.C., Kimball, J.S., et al., 2020. Recent amplified global gross primary productivity due to temperature increase is offset by reduced productivity due to water constraints. *AGU Adv.* 1, e2020AV000180 <https://doi.org/10.1029/2020AV000180>.
- Marshall, V.M., Lewis, M.M., Ostendorf, B., 2012. Buffel grass (*Cenchrus ciliaris*) as an invader and threat to biodiversity in arid environments: a review. *J. Arid Environ.* 78, 1–12.
- McKenzie, D., Littell, J.S., 2017. Climate change and the eco-hydrology of fire: will area burned increase in a warming western USA. *Ecol. Appl.* 27, 26–36. <https://doi.org/10.1002/eap.1420>.
- McLaughlin, S.P., Bowers, J.E., 1982. Effects of wildfire on a Sonoran Desert plant community. *Ecology* 246–248.
- Miettinen, J., Shi, C., Liew, S.C., 2012. Two decades of destruction in Southeast Asia's peat swamp forests. *Front. Ecol. Environ.* 10, 124–128. <https://doi.org/10.1890/100236>.
- Monzón-Alvarado, C., Waylen, P., Keys, E., 2014. Fire management and climate variability: challenges in designing environmental regulations. *Land Use Pol.* 39, 12–21. <https://doi.org/10.1016/j.landusepol.2014.03.003>.
- Morton, D.C., DeFries, R.S., Shimabukuro, Y.E., et al., 2006. Cropland expansion changes deforestation dynamics in the southern Brazilian Amazon. *Proc. Natl. Acad. Sci. U. S. A.* 103, 14637–14641. <https://doi.org/10.1073/pnas.0606377103>.
- Mouillot, F., Rambal, S., Richard, J., 2002. Simulating climate change impacts on fire frequency and vegetation dynamics in a Mediterranean-type ecosystem. *Global Change Biol.* 8, 423–437.
- Murdiyarso, D., Lebel, L., Gintings, A.N., et al., 2004. Policy responses to complex environmental problems: insights from a science-policy activity on transboundary haze from vegetation fires in Southeast Asia. *Agric. Ecosyst. Environ.* 104, 47–56. <https://doi.org/10.1016/j.agee.2004.01.005>.
- Page, S.E., Siegert, F., Rieley, J.O., et al., 2002. The amount of carbon released from peat and forest fires in Indonesia during 1997. *Nature* 420, 61–65. <https://doi.org/10.1038/nature01141.1>.
- Patra, P.K., Ishizawa, M., Maksyutov, S., et al., 2005. Role of biomass burning and climate anomalies for land-atmosphere carbon fluxes based on inverse modeling of atmospheric CO<sub>2</sub>. *Global Biogeochem. Cycles* 19, 1–10. <https://doi.org/10.1029/2004GB002258>.
- Piao, S., Wang, X., Wang, K., et al., 2020. Interannual variation of terrestrial carbon cycle: issues and perspectives. *Global Change Biol.* 26, 300–318.
- Pilliod, D.S., Welty, J.L., Arkle, R.S., 2017. Refining the cheatgrass–fire cycle in the Great Basin: precipitation timing and fine fuel composition predict wildfire trends. *Ecol. Evol.* 7, 8126–8151. <https://doi.org/10.1002/ece3.3414>.
- Pinzon, J.E., Tucker, C.J., 2014. A non-stationary 1981–2012 AVHRR NDVI3g time series. *Rem. Sens.* 6, 6929–6960. <https://doi.org/10.3390/rs6086929>.
- Rabin, S.S., Melton, J.R., Lasslop, G., et al., 2017. The Fire Modeling Intercomparison Project (FireMIP), phase 1: experimental and analytical protocols with detailed model descriptions. *Geosci. Model Dev. (GMD)* 10, 1175–1197. <https://doi.org/10.5194/gmd-10-1175-2017>.
- Ramankutty, N., Evan, A.T., Monfreda, C., et al., 2008. Farming the planet: 1. geographic distribution of global agricultural lands in the year 2000. *Global Biogeochem. Cycles* 22, 1–19. <https://doi.org/10.1029/2007GB002952>.
- Randerson, J.T., Chen, Y., van der Werf, G.R., et al., 2012. Global burned area and biomass burning emissions from small fires. *J. Geophys. Res.* G Biogeosci. 117, 1–23. <https://doi.org/10.1029/2012JG002128>.
- Randerson, J.T., van der Werf, G.R., Giglio, L., et al., 2015. Global fire emissions database, version 4.1 (GFEDv4). ORNL DAAC.

- Rao, L.E., Allen, E.B., 2010. Combined effects of precipitation and nitrogen deposition on native and invasive winter annual production in California deserts. *Oecologia* 162, 1035–1046. <https://doi.org/10.1007/s00442-009-1516-5>.
- Romero-Ruiz, M., Etter, A., Sarmiento, A., et al., 2010. Spatial and temporal variability of fires in relation to ecosystems, land tenure and rainfall in savannas of northern South America. *Global Change Biol.* 16, 2013–2023. <https://doi.org/10.1111/j.1365-2486.2009.02081.x>.
- Setterfield, S.A., Rossiter-Rachor, N.A., Hutley, L.B., et al., 2010. Biodiversity research: turning up the heat: the impacts of *Andropogon gayanus* (gamba grass) invasion on fire behaviour in northern Australian savannas. *Divers. Distrib.* 16, 854–861.
- Shakesby, R.A., 2011. Post-wildfire soil erosion in the Mediterranean: review and future research directions. *Earth Sci. Rev.* 105, 71–100. <https://doi.org/10.1016/j.earscirev.2011.01.001>.
- Shea, R.W., Shea, B.W., Kauffman, J.B., et al., 1996. Fuel biomass and combustion factors associated with fires in savanna ecosystems of South Africa and Zambia. *J. Geophys. Res. Atmos.* 101, 23551–23568. <https://doi.org/10.1029/95jd02047>.
- Song, B., Niu, S., Wan, S., 2016. Precipitation regulates plant gas exchange and its long-term response to climate change in a temperate grassland. *J. Plant Ecol.* 9, 531–541. <https://doi.org/10.1093/jpe/rtw010>.
- Sun, Z., Wang, X., Zhang, X., et al., 2019. Evaluating and comparing remote sensing terrestrial GPP models for their response to climate variability and CO<sub>2</sub> trends. *Sci. Total Environ.* 668, 696–713. <https://doi.org/10.1016/j.scitotenv.2019.03.025>.
- Thonicke, K., Spessa, A., Prentice, I.C., et al., 2010. The influence of vegetation, fire spread and fire behaviour on biomass burning and trace gas emissions: results from a process-based model. *Biogeosciences* 7, 1991–2011. <https://doi.org/10.5194/bg-7-1991-2010>.
- Urbieto, I.R., Zavala, G., Bedia, J., et al., 2015. Fire activity as a function of fire-weather seasonal severity and antecedent climate across spatial scales in southern Europe and Pacific western USA. *Environ. Res. Lett.* 10 <https://doi.org/10.1088/1748-9326/10/11/114013>.
- van den Hurk, B., Kim, H., Krinner, G., et al., 2016. LS3MIP (v1.0) contribution to CMIP6: the Land Surface, Snow and Soil moisture Model Intercomparison Project: aims, setup and expected outcome. *Geosci. Model Dev.* 9, 2809–2832. <https://doi.org/10.5194/gmd-9-2809-2016>.
- van der Werf, G.R., Randerson, J.T., Giglio, L., et al., 2006. Interannual variability in global biomass burning emissions from 1997 to 2004. *Atmos. Chem. Phys.* 6, 3423–3441. <https://doi.org/10.5194/acp-6-3423-2006>.
- van der Werf, G.R., Dempewolf, J., Trigg, S.N., et al., 2008a. Climate regulation of fire emissions and deforestation in equatorial Asia. *Proc. Natl. Acad. Sci. U. S. A.* 105, 20350–20355. <https://doi.org/10.1073/pnas.0803375105>.
- van der Werf, G.R., Randerson, J.T., Giglio, L., et al., 2008b. Climate controls on the variability of fires in the tropics and subtropics. *Global Biogeochem. Cycles* 22, 1–13. <https://doi.org/10.1029/2007GB003122>.
- van Wilgen, B.W., 2009. The evolution of fire and invasive alien plant management practices in fynbos. *South Afr. J. Sci.* 105, 335–342. <https://doi.org/10.4102/sajs.v105i9.10.106>.
- Vargas, R., Collins, S.L., Thomey, M.L., et al., 2012. Precipitation variability and fire influence the temporal dynamics of soil CO<sub>2</sub> efflux in an arid grassland. *Global Change Biol.* 18, 1401–1411. <https://doi.org/10.1111/j.1365-2486.2011.02628.x>.
- Wei, F., Wang, S., Fu, B., et al., 2020. Nonlinear dynamics of fires in Africa over recent decades controlled by precipitation. *Global Change Biol.* 26, 4495–4505. <https://doi.org/10.1111/gcb.15190>.
- Wieder, R.K., Vitt, D.H., 2006. *Boreal peatland ecosystems*. Springer Science & Business Media.
- Wright, H.A., 1980. *The role and use of fire in the semidesert grass-shrub type*. Department of Agriculture, Forest Service, Intermountain Forest and Range.
- Xu, X., Jia, G., Zhang, X., et al., 2020. Climate regime shift and forest loss amplify fire in Amazonian forests. *Global Change Biol.* 26, 5874–5885. <https://doi.org/10.1111/gcb.15279>.
- Yin, Y., Ciais, P., Chevallier, F., et al., 2016. Variability of fire carbon emissions in equatorial Asia and its nonlinear sensitivity to El Niño. *Geophys. Res. Lett.* 43, 10,472–10,479. <https://doi.org/10.1002/2016GL070971>.